



Cite this: *Phys. Chem. Chem. Phys.*, 2019, 21, 6171

Manipulation of dipolar magnetism in low-dimensional iron oxide nanoparticle assemblies

Li-Ming Wang,^{id} *^{abc} Asma Qdemat,^a Oleg Petravic,^a Emmanuel Kentzinger,^a Ulrich Rücker,^a Fengshan Zheng,^d Peng-Han Lu,^d Xian-Kui Wei,^d Rafal E. Dunin-Borkowski^d and Thomas Brückel^a

The manipulation of magnetic states in nanoparticle supercrystals promises new pathways to design nanocrystalline magnetic materials and devices. Trench-patterned silicon substrates were used as templates to guide the self-assembly of iron oxide nanoparticles. Grazing incidence small angle X-ray scattering shows that the nanoparticles form a long-range ordered structure along the trench direction while in the direction perpendicular to the trenches, no coherent structure is observable. Electron holography provides evidence of an ordered magnetic state of nanoparticle moments in the remanent state after the application of a saturation magnetic field parallel to the trenches. However, a disordered magnetic state was observed in a perpendicular geometry. Hysteresis loops indicate that the nanoparticle moments form a superferromagnetic state for the geometry parallel to the trenches. Memory effect investigations reveal that the disordered magnetic state corresponds to a collective superspin glass state in the perpendicular geometry, while the superferromagnetic state in the parallel geometry suppresses the superspin glass state.

Received 17th January 2019,
Accepted 25th February 2019

DOI: 10.1039/c9cp00302a

rsc.li/pccp

Arrays of nanoparticles (NPs) have unique potential applications, in photonics, spintronics and as novel nanomaterials.^{1–5} Magnetic NPs, as building blocks inside self-organized one-, two- or three-dimensional arrangements are candidates for *e.g.* high-density data storage media or multifunctional spintronic devices.^{6,7}

For applications, long-range ordered NP arrays are often required for the fabrication of devices with tunable properties.^{8–10} Recently, a rich variety of methods have been reported for depositing colloidal NPs onto patterned surfaces into long-range ordered nanostructures.^{11–14} Among these methods, spin-coating is widely used as a convenient and fast technique. For example, D. Xia *et al.* demonstrated directed self-assembly of silicon NPs into nanoscale-groove patterned surfaces using the spin-coating method.¹⁴

Self-assembled NPs also constitute model systems for the fundamental understanding of nanomaterials in comparison to conventional materials. One example is dipolar magnetism.¹⁵ The energy of two magnetic dipoles $\vec{\mu}_i$ and $\vec{\mu}_j$ separated by \vec{r}_{ij} is: $E_{dd} = (\vec{\mu}_i \cdot \vec{\mu}_j - 3(\vec{\mu}_i \cdot \hat{r}_{ij})(\vec{\mu}_j \cdot \hat{r}_{ij}))\mu_0/4\pi r_{ij}^3$. In conventional

materials, where atomic magnetic moments sit on crystallographic lattice sites, the temperature equivalent of this energy is in the order of 1 K and hence often mostly irrelevant for the magnetic order such as ferro- or antiferromagnetism. However, considering NPs as building blocks instead of atoms, the dipolar interaction energy can be orders of magnitude larger. For example, two iron oxide NPs with a diameter of 20 nm and hence with a magnetic moment μ of $3 \times 10^6 \mu_B$ being in close contact experience a dipolar interaction energy of around $2100k_B T$. Increasing the NP separation can lead to drastic changes of the dipolar energy, *e.g.* it is reduced to $135k_B T$ for a separation of $r_{ij} = 50$ nm, and to $5k_B T$ for $r_{ij} = 150$ nm.

Dipolar interactions between NPs can lead to collective states like glassy behavior, superspin-glass (SSG) behavior or superferromagnetism (SFM) depending on the distance and spatial arrangement of the NPs.^{5,16,17} A recent study showed that switching of the magnetic properties of Ni nanocrystals between a superparamagnetic and a stable superferromagnetic state was realized *via* the magneto-electric coupling by applying an electric field to the sample.¹⁸ Other studies demonstrated the switching of the magnetic state by application of light.¹⁹ To our knowledge, only either a SSG or a SFM state is found in one system. Here, we report on the experimental demonstration of switching between a SFM and a SSG state depending on the orientation of the magnetic field in a system of self-assembled iron oxide NPs. Hereby the NPs are arranged as

^a Jülich Centre for Neutron Science JCNS and Peter Grünberg Institut PGI, JARA-FIT, Forschungszentrum Jülich GmbH, 52425, Jülich, Germany

^b Institute of High Energy Physics, Chinese Academy of Sciences, Beijing 100049, China. E-mail: wanglm@ihep.ac.cn; Tel: +86 0769 89254869

^c Dongguan Neutron Science Center, Dongguan 523803, China

^d Ernst Ruska-Centre for Microscopy and Spectroscopy with Electrons and Peter Grünberg Institute, Forschungszentrum Jülich GmbH, 52425 Jülich, Germany

quasi one-dimensional chains inside trenches which were prepared by imprint lithography.

1 Experimental

We use commercially available oleic acid coated iron oxide NPs dispersed in toluene (Ocean NanoTech). The spherical particles have a mean diameter of 20 nm and a size distribution of 7%. We choose 20 nm iron oxide nanoparticles, because 20 nm is well below the critical single-domain diameter of iron oxide nanoparticles. For these sizes the assumption of a magnetic mono-domain switching is usually assumed to hold. In each particle, consisting mainly of maghemite, there is a fraction of AF wuestite.^{6,20,21} We assume that these fractions of wuestite will alter the particle magnetism internally, but due to the small size (being well below the single-domain diameter) no fragmentation or multi-domain state is expected.^{22,23} On the other hand the size of 20 nm is large enough to be easily observed by SEM and e-Holography methods. $5 \times 5 \times 0.5 \text{ mm}^3$ trench patterned silicon substrates (Eulitha company) were used to guide the self-assembly of NPs. The trench pattern completely covers the substrate and was fabricated with a width of 150 nm, a depth of 100 nm and a pitch of 300 nm using the displacement talbot lithography method.²⁴

The NPs dispersed in toluene have an initial concentration of 25 mg mL^{-1} and were diluted with toluene in the volume ratio of 1:10. Afterwards, the diluted dispersion was placed into an ultra-sonic bath with an operating frequency of 5 kHz for 5 min to homogeneously disperse the NPs. $3 \mu\text{L}$ of solution was taken by a pipette to drop onto the $5 \times 5 \times 0.5 \text{ mm}^3$ silicon substrates which was fixed onto a spin coater *via* a vacuum pipe. Immediately after application of the droplet the spin coater was kept running at the speed of 3000 rpm for 60 s.

To improve the assembly of the NPs in the trenches, the as-prepared samples were placed in a container with a pair of permanent magnets at both sides. The magnetic field was applied perpendicular to the trench direction. In addition, $1 \mu\text{L}$ toluene was added onto the substrate surface 10 times every 3 min. This specific procedure iteratively redisperses the fixed NPs and moves them to produce an improved order. Such a redispersion has a similar role to post-annealing of bulk crystals to heal defects.

The micromorphology of the NPs was studied using a scanning electron microscope (SEM, SU8000 from Hitachi). Magnetometry measurements were performed using a superconducting quantum interference device magnetometer (SQUID, MPMS XL from Quantum Design). The temperature ranges from 1.7 to 400 K with a resolution of 0.1 K at the sample position. The lateral coherent structure of our NPs was characterized using the in-house high-brilliance grazing incidence small angle X-ray scattering GISAXS/SAXS instrument GALAXI ($\lambda = 1.34 \text{ \AA}$).²⁵ The magnetic phase map of NPs was studied using off-axis electron holography in a transmission electron microscope (TEM) at 300 kV operated in field-free condition (Lorentz mode). Holograms were recorded at room temperature after an external magnetic field application of 0.98 T and -0.98 T parallel or perpendicular to the trench direction by a pair of permanent magnets, respectively. The phase is sensitive to the in-plane component of the magnetic induction integration along the electron beam direction and to the electrostatic mean inner potential. The mean inner potential contribution was removed by subtracting the two holograms with the magnetization of NPs reversed by using the magnets.²⁶

2 Results and discussion

The SEM image of the trench-patterned silicon substrates is displayed in Fig. 1(a). After spin-coating and redispersion of NPs onto the substrates, the NPs are located inside the trenches with very few particles on top of the mesa as can be seen from Fig. 1(b). The NPs show a continuous close-packing with a width of approx. 6 to 7 particles across one trench.

In order to study the structural coherence of the NPs inside the trenches, GISAXS measurements were performed with the incident beam perpendicular to the trench direction, corresponding to an azimuthal angle of 90° (Fig. 2(a)). The incident angle with respect to the substrate surface was $\alpha_i = 0.18^\circ$. Intensity dots superimposed to the rings are observed. The 2d-Bragg dots along Q_y are due to the laterally correlated NP arrangement while the dots along Q_z provide information on the out-of-plane coherent structure.

A line cut along Q_y at $Q_z = 0.35 \text{ nm}^{-1}$ was taken from the GISAXS pattern. Bragg peaks at $Q_y = 0.28 \text{ nm}^{-1}$, 0.58 nm^{-1} and 0.91 nm^{-1} can be observed as shown in Fig. 2(b). The peaks are indexed assuming a hexagonal close-packed lattice with a lattice constant $a = 21.03 \pm 0.53 \text{ nm}$. This value fits well to the average NP distance as found from the SEM studies. After taking the instrument resolution into account, a Lorentzian profile is used to fit to the second order peaks at $Q_y = 0.58 \text{ nm}^{-1}$ and -0.58 nm^{-1} which yields a structural coherence length of $60.50 \pm 0.90 \text{ nm}$.

GISAXS cannot provide information about the NP coherent order perpendicular to the trench axis, as explained in the appendix. Moreover, it can be expected there is no long-ranged coherent structure of the NPs between the trenches since NPs ordering in one trench is independent from the other ones.

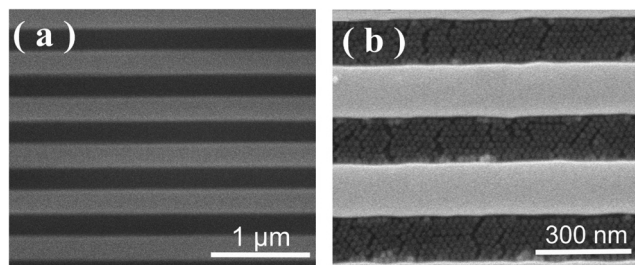


Fig. 1 SEM image of (a) trench-patterned silicon substrates. (b) Self-assembled NPs on the trench-patterned silicon substrates.

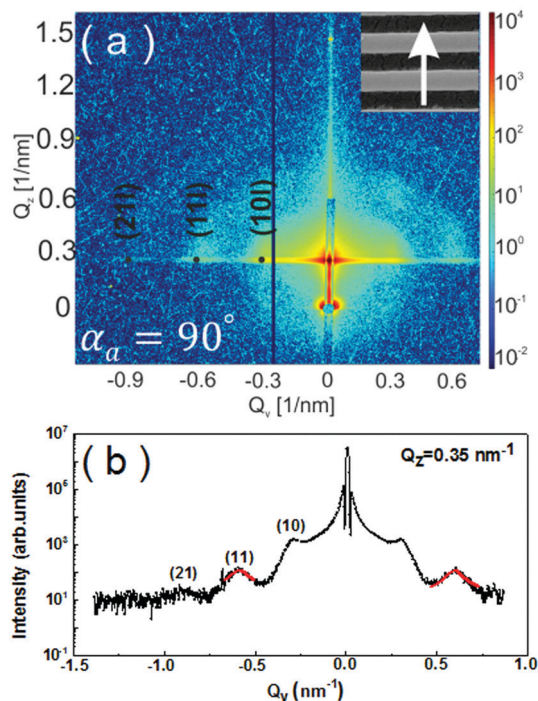


Fig. 2 (a) GISAXS pattern of the sample with the beam perpendicular to the trench direction. The azimuthal angle (α_a) of the sample was 90° . The angle of the incident beam (α_i) with respect to the substrate surface is 0.18° . The black line is due to a dead region of the detector. The direction of the X-ray beam with respect to the trenches is illustrated at the top-right corner. (b) Line cut along Q_y at $Q_z = 0.35 \text{ nm}^{-1}$ with a Lorentzian fit (red line) of the two (11) Bragg peaks. The Bragg peaks were indexed according to a hexagonal lattice with $a = 21 \pm 0.53 \text{ nm}$.

Magnetization hysteresis loops were measured with an external magnetic field applied parallel to the trench direction at 300 K and subsequently at 10 K. Afterwards, the sample was rotated to orient the field perpendicular to the trench direction and the same measurement sequence was performed. The results compared for different field directions at 300 K and 10 K are shown in Fig. 3(a) and (b), respectively.

The magnetization with the magnetic field applied perpendicular to the trench direction shows a harder magnetic behavior than for the parallel case. The difference can be quantified by the magnetic squareness ζ which is expressed as the ratio of

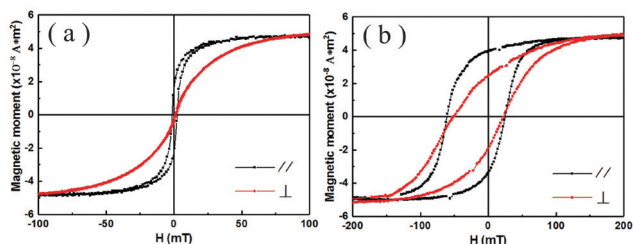


Fig. 3 Hysteresis loops for NPs on a patterned silicon substrate (a) at 300 K and (b) at 10 K. The black hysteresis loops in both figures were measured with the field applied parallel to the trench direction and the red ones were measured with the field perpendicular to the trench direction.

the remanent magnetization (M_r) to the saturation magnetization (M_s), *i.e.* $\zeta = M_r/M_s$. The magnetic squareness is a widely used criteria for the evaluation of magnetic anisotropy and of the magnetization reversal mode.²⁷ Here, we assume that the reversal mode inside the NPs is coherent rotation in all cases,⁵ hence the squareness value will provide the information only about a change of anisotropy. Note both figures were reproducible from control measurements in order to verify that no artifact occurred.

M_r at both temperatures are significantly larger in the parallel case than for the perpendicular case while the M_s are identical at both directions. Hence, ζ is increased by 589% and 61% at 300 K and 10 K, respectively for the parallel configuration. The increase of ζ can be interpreted by the shape anisotropy of the quasi one-dimensional NP arrangement. One such NP chain can be approximated as a homogeneous magnetic sample in the form of a rod. Such a rod exhibits a demagnetization factor $N_{\parallel} = 0$ along the rod axis and $N_{\perp} = 1/2$ along the two perpendicular directions. Hereby a shape induced magnetic easy axis along the rod is formed.^{28–30}

According to the dipolar energy between two magnetic dipoles mentioned in the introduction part, the dipolar energy favors the magnetic moments to align in the form of a head-to-tail arrangement.³¹ If the particles are ordered in a chain like structure then such a head-to-tail arrangement is energetically more favorable. Hence, the overall effect is that a magnetic anisotropy is induced which resembles the magnetic shape-anisotropy as known from homogeneously filled objects.³² The scenario is also evidenced in previous experimental results.³³ For example, T. Wen *et al.* reported that 10 nm Fe_3O_4 NPs in a one dimensional structure tend to orient with their superspins in a head-to-tail configuration with their easy axis aligned with the applied field.³⁴ SFM dipolar interactions in hexagonal patterned spherical NPs are evidenced by electron holography by M. Varón *et al.*³¹

Shape anisotropy also gives rise to an energy barrier in the superspin reversal process. As shown in Fig. 3(a) and (b), a larger coercive field is needed to reverse the superspins when the magnetic field is parallel to the trench direction. The coercive field increases by 105% and 18% at 300 K and 10 K from the perpendicular to parallel geometry, respectively.

In addition, an exchange bias (EB) effect is observed at 10 K, in both hysteresis loops as shown in Fig. 3(b). It is due to the exchange coupling effect in the multi-component NPs, consisting of ferrimagnetic maghemite and antiferromagnetic wuestite with the Néel temperature of 198 K.²⁰

In order to visualize the magnetic structure of the NP chains, off-axis electron holography in a transmission electron microscope was employed to directly probe the magnetic phase of the self-assembled NPs in the trenches at their remanent state.

Fig. 4(a) shows the morphology of the self-assembled NPs in a trench. Fig. 4(b) shows a uniform holographic phase map, which was obtained at the remanent state after application of a magnetic field of 0.98 T perpendicular to the trench direction as indicated by the black arrow. The projected in-plane magnetic induction (Fig. 4(c)) was calculated from the gradient of

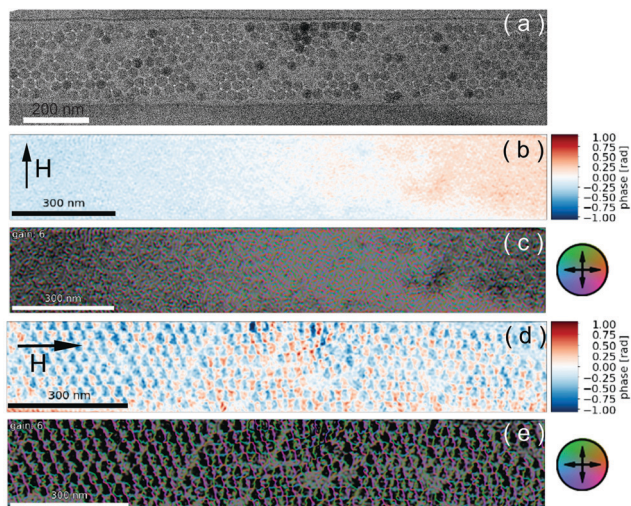


Fig. 4 (a) Bright-field TEM image of the NPs in a randomly-chosen trench. (b and d) Magnetic phase images of NPs at the remanent state after application of a magnetic field of 0.98 T perpendicular and parallel to the trenches, respectively. The scale bar of the magnetic phase is indicated at the right hand side. (c and e) The projected in-plane magnetic induction maps of the NPs corresponding to (b and d), respectively. Colors and arrows are used to indicate both the strength and the direction of the projected in-plane magnetic induction as shown by the color wheel on the right hand side.

the phase image. The uniform contrast over the entire trench implies that there is no overall ordered magnetic structure in this state.

Analogously, after a magnetic field of 0.98 T was applied parallel to the trench direction, the magnetic phase of NPs at the remanent state was measured and the projected in-plane magnetic induction was calculated as shown in Fig. 4(d) and (e), respectively. The periodic contrast in both phase image and magnetic induction map indicates that there is an ordered magnetic structure between the NPs. It reveals that a net magnetic moment is induced at the remanent state which is very likely due to a coherent NP structure in this direction. It is worth noting that the direction of the magnetic induction is inclined to the trench, which may be due to charging effects from the oxide layers on the surface of the semiconducting substrate.^{35,36}

With the magnetic field applied parallel or perpendicular to the trench direction temperature dependent magnetometry measurements were performed (Fig. 5). The sample was first cooled in zero magnetic field from room temperature down to 5 K. Subsequently a constant field of 5 mT was applied and the ZFC curve recorded upon warming up to 350 K. Finally the FC measurement was performed at the same field upon cooling. The procedures were repeated for a field of 20 mT and once for the field parallel and once for the field perpendicular to the trenches. It is expected that at the same field value, the magnetization measured with the field direction parallel to the trench direction is larger than perpendicular due to the energetically more favorable superspin alignment along the parallel direction.

In the ZFC curve the peak temperature T_P is defined as the first zero value of the differential curve of the ZFC magnetic moment

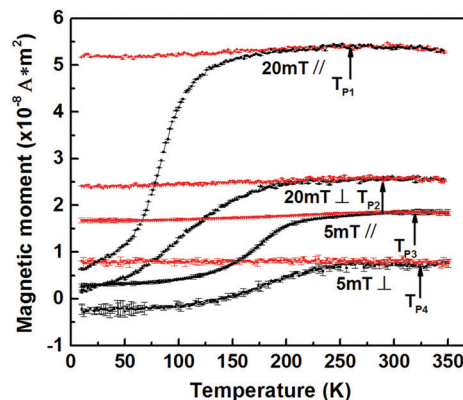


Fig. 5 Temperature dependence of the magnetic moment of NPs self-assembled in trenches patterned Si substrate during zero field cooling (ZFC, black) and field cooling (FC, red) at the magnetic field of 20 mT and 5 mT. The magnetic field was applied along and perpendicular to the trenches. The peak temperature T_P was defined as the first zero value of the derivation of the ZFC magnetization.

from the low temperature side. In SPM systems T_P corresponds to the blocking temperature T_B . However, in collective systems as SSG systems it corresponds to a collective freezing temperature.

Firstly, one finds that for both geometries the peak temperature shifts to smaller values with increasing applied field. This is expected from SPM-like systems as an increased field reduces the effective relaxation time scale.^{37–39}

Secondly, the amplitude of the magnetic moment is larger for the parallel geometry compared to the perpendicular one for both fields. This corresponds to the fact that a ferromagnetic-like ordered arrangement of superspins in the parallel geometry will show a larger moment along the shape anisotropy axis at the same field and temperature compared to the perpendicular case. Hereby one should note that the negative value of the ZFC curve at low temperatures measured perpendicularly at 5 mT is due to the diamagnetic signal of the silicon substrate overcompensating the positive moment from the NPs.

While the regular ZFC–FC curves do not provide further insight into the magnetic properties of the system, measurements of the magnetic memory effect provide direct information on a possible collective state. The presence of a non-vanishing memory effect is a direct evidence for a SSG state.^{17,40,41}

Curves of the memory effect for the two field geometries are shown in Fig. 6. Firstly, a regular ZFC curve was measured as a reference measurement at a magnetic field of 5 mT. Subsequently, the sample was again cooled from 300 K in zero field with a temporary pause at a temperature T_S ($< T_P$) for $t_s = 7200$ s. Then the cooling was resumed down to 5 K and the magnetic moment ($m_{\text{aging}}^{\text{ZFC}}$) was measured during heating in a field of 5 mT analogous to the reference curve. Such ZFC curves measured in parallel geometry with $T_S = 140$ K, 160 K and 190 K are shown in the upper part of Fig. 6(a), while the difference Δm is shown in the lower part corresponding to the right Y-axis. The aged ZFC curves coincide with the regular ZFC curve below and above T_S . In the difference curve Δm , only a small bump is found near T_S (Fig. 6(a)).

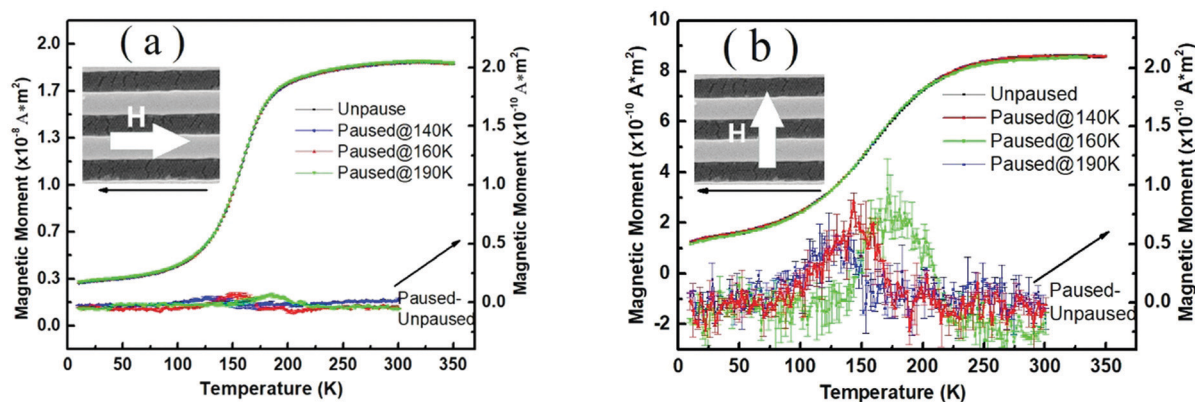


Fig. 6 Regular ZFC curves and ZFC curves obtained with an aging stop at 140 K and in addition independent measurements at 160 K and 190 K, respectively. The value of the magnetic moment for the ZFC curves is indicated in the left Y axis while the right hand Y axis corresponds to the subtraction between paused ZFC and regular ZFC curves. The color of the subtracted curves is the same as the corresponding ZFC curves. (a) Measurement with the field applied parallel to the trench direction, as shown in the inset, and (b) with the field applied perpendicular to the trench direction, as indicated in the inset.

The situation is different when measuring the memory effect in the perpendicular geometry. Here the Δm is larger by a factor of 10 compared to the parallel case. This indicates, that in the perpendicular geometry the memory effect is clearly more pronounced and consequently the SSG state is more pronounced than in the parallel case.

The observation can be understood in the following way: for the parallel geometry the shape anisotropy of the chain-like NP arrangement favors a SFM alignment of the superspins. Such an ordered state will not show significant frustration effects and consequently no or less SSG behavior. In contrast, in the perpendicular geometry the competition of inter-particle dipole-dipole interactions, individual NP anisotropy directions, the shape anisotropy of the chain-like arrangement and the Zeeman energy due to the applied field along the hard axis of the chains will lead to frustration. No ordered state is observed and instead a SSG behavior is found as clearly evidenced by the magnetic memory effect.^{41,42}

3 Conclusions

In summary, we have presented a simple approach for the templated assembly of iron oxide NPs into pseudo-1D NP patterns on trench patterned silicon substrates. A NP coherent structure and magnetic correlations along the trench direction can be observed using GISAXS and electron holography, respectively. In contrast, in the direction perpendicular to the trench direction, no ordered magnetic correlations are observable. Memory effect measurements reveal that the emerging SFM order for the parallel geometry suppresses a SSG state while a SSG state dominates in the perpendicular geometry. With other words, the collective magnetic state of the system can be manipulated by only varying the field geometry. Our work provides the possibility to design novel tunable magnetic devices.

Conflicts of interest

There are no conflicts to declare.

Appendix

Fig. 7(a) shows a GISAXS pattern measured with the incoming beam parallel to the trench direction. For this case, the angle of the incident beam with respect to the trench direction was $\alpha_a = 0.3^\circ$. This titled azimuthal angle prevents too large scattering background from the trenches overwhelming the intensities from

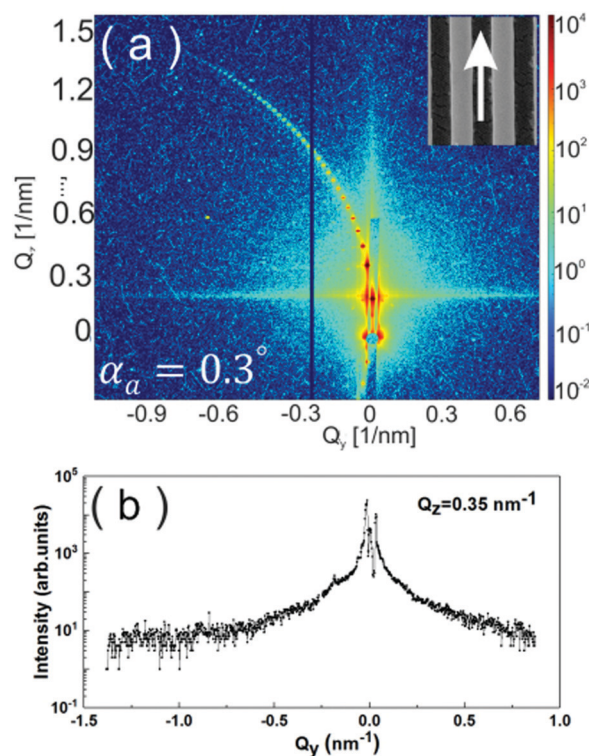


Fig. 7 (a) GISAXS pattern of the sample with the beam almost parallel to the trench direction. The angle of the incident beam (α_i) with respect to the substrate surface is 0.18° . The azimuthal angle (α_a) of the sample was titled by 0.3° to reduce the scattering intensity from the trenches. The direction of the X-ray beam with respect to the trenches is illustrated at the top-right corner. (b) Line cut from (a) along Q_y at $Q_z = 0.35 \text{ nm}^{-1}$.

the NPs. The visible semicircle in (a) is a result of the structure factor of the trenches. Apart from the circle, only blurry rings around specular reflex are observed which are due to scattering by surface and interface roughness.

The absence of Bragg peaks, even for a coherent arrangement of NP along the Q_y -direction perpendicular to the stripes, can be explained in the following way. The NP arrangement along that direction can be described by the product of a non-disrupted periodic NP arrangement and a periodically stepped function of period given by the pitch of the patterned substrate. The scattering amplitude along the Q_y -direction is proportional to the Fourier transform of the dependency along the y -direction of the X-ray-matter interaction potential corresponding to this NP arrangement. It is known that the Fourier transform of the product of two functions equals the convolution product of the Fourier transforms of the individual functions. The Q_y -dependency of the total scattering amplitude is therefore the convolution product of the scattering amplitude due to the non-disrupted periodic NP arrangement and the scattering amplitude of the lithographic pattern, oscillating around 0. As the pitch of the patterned substrate is much larger than the NP periodicity along the y -direction, the total scattering amplitude is 0. Hence, even if there is coherent order of the NP perpendicular to the stripes, one cannot observe any Bragg peak.

Acknowledgements

Financial support from China Scholarship Council (CSC) is gratefully acknowledged. We thank Prof. R. Waser (PGI-7) for the opportunity to use their SEM. We would like to thank Prof. C. Schneider (PGI-6) for providing us the opportunity to use their equipments. We also thank Jochen Friedrich and Berthold Schmitz for technical support.

References

- H. T. Rekola, T. K. Hakala and P. Tóormá, *ACS Photonics*, 2018, **5**, 1822–1826.
- W. Kleemann and C. Binek, in *Multiferroic and magneto-electric materials, Magnetic Nanostructures*, ed. H. Zabel and M. Farle, Springer, Berlin Heidelberg, 2013, vol. 246.
- K. Saha, M. Rahimi, M. Yazdani, S. T. Kim, D. F. Moyano, S. Hou, R. Das, R. Mout, F. Rezaee and M. Mahmoudi, *et al.*, *ACS Nano*, 2016, **10**, 4421–4430.
- A. Dong, J. Chen, P. M. Vora, J. M. Kikkawa and C. B. Murray, *Nature*, 2010, **466**, 474.
- S. Bedanta, O. Petravic and W. Kleemann, Supermagnetism, in *Handbook of Magnetic Materials*, ed. K. J. H. Buschow, Elsevier, 2015, vol. 23.
- L.-M. Wang, O. Petravic, E. Kentzinger, U. Rücker, S. Markus, X.-K. Wei, M. Heggen and T. Brückel, *Nanoscale*, 2017, **9**, 12957.
- J. Krempaský, S. Muff, F. Bisti, M. Fanciulli, H. Volfová, A. P. Weber, N. Pilet, P. Warnicke, H. Ebert and J. Braun, *et al.*, *Nat. Commun.*, 2016, **7**, 13071.
- T. Ozdemir, D. Sandal, M. Culha, A. Sanyal, N. Z. Atay and S. Bucak, *Nanotechnology*, 2010, **21**, 125603.
- D. Lisjak, P. Jenus and A. Mertelj, *Langmuir*, 2014, **30**, 6588.
- L. Hongcheng, Y. Takafumi, Y. Wataru, H. Naoaki, K. Yoji, A. Yoshitami and K. Hiroshi, *J. Am. Chem. Soc.*, 2015, **137**, 9804–9807.
- X. Fan, Q. Hao, R. Jin, H. Huang, Z. Luo, X. Yang, Y. Chen, X. Han, M. Sun and Q. Jing, *et al.*, *Sci. Rep.*, 2017, **7**, 2322.
- Y.-J. Oh, C. A. Ross, Y. S. Jung, Y. Wang and C. V. Thompson, *Small*, 2009, **5**, 860.
- Y. Lee, H. Lee, P. B. Messersmith and T. G. Park, *Macromol. Rapid Commun.*, 2010, **31**, 2109.
- D. Xia, A. Biswas, D. Li and S. R. Brueck, *Adv. Mater.*, 2004, **16**, 1427.
- D. V. Talapin, E. V. Shevchenko, C. B. Murray, A. V. Titov and P. Král, *Nano Lett.*, 2007, **7**, 1213.
- M. Varón, M. Beleggia, T. Kasama, R. J. Harrison, R. E. Dunin-Borkowski, V. F. Puentes and C. Frandsen, *Sci. Rep.*, 2013, **3**, 1234.
- O. Petravic, *Superlattices Microstruct.*, 2010, **47**, 569.
- H. K. Kim, L. T. Schelhas, S. Keller, J. L. Hockel, S. H. Tolbert and G. P. Carman, *Nano Lett.*, 2013, **13**, 884–888.
- S.-i. Ohkoshi, K. Imoto, Y. Tsunobuchi, S. Takano and H. Tokoro, *Nat. Chem.*, 2011, **3**, 564.
- M. Benitez, D. Mishra, P. Szary, G. B. Confalonieri, M. Feyen, A. Lu, L. Agudo, G. Eggeler, O. Petravic and H. Zabel, *J. Phys.: Condens. Matter*, 2011, **23**, 126003.
- L.-M. Wang, O. Petravic, S. Mattauch, A. Koutsoumbas, X.-K. Wei, M. Heggen, V. Leffler, S. Ehlert and T. Brückel, *J. Phys. D: Appl. Phys.*, 2018, **52**, 065301.
- A.-H. Lu, E. E. Salabas and F. Schüth, *Angew. Chem., Int. Ed.*, 2007, **46**, 1222–1244.
- S. Singamaneni, V. N. Bliznyuk, C. Binek and E. Y. Tsybal, *J. Mater. Chem.*, 2011, **21**, 16819.
- H. H. Solak, C. Dais and F. Clube, *Opt. Express*, 2011, **19**, 10686.
- Jülich Center for Neutron Science, GALAXI: Gallium anode low-angle X-ray instrument, 2016 *Journal of large-scale research facilities JLSRF*, **2**, A61, , DOI: 10.17815/jlsrf-2-109.
- R. E. Dunin-Borkowski, M. R. McCartney, R. B. Frankel, D. A. Bazylinski, M. Pósfai and P. R. Buseck, *Science*, 1998, **282**, 1868.
- R. McCurrie and G. Carswell, *Philos. Mag.*, 1971, **23**, 333.
- K. Butter, P. Bomans, P. Frederik, G. Vroege and A. Philipse, *Nat. Mater.*, 2003, **2**, 88.
- J. Ku, D. M. Aruguete, A. P. Alivisatos and P. L. Geissler, *J. Am. Chem. Soc.*, 2010, **133**, 838.
- V. Salgueiriño-Maceira, M. A. Correa-Duarte, A. Hucht and M. Farle, *J. Magn. Magn. Mater.*, 2006, **303**, 163.
- M. Varón, M. Beleggia, T. Kasama, R. Harrison, R. Dunin-Borkowski, V. Puentes and C. Frandsen, *Sci. Rep.*, 2013, **3**, 1234.
- J. Osborn, *Phys. Rev.*, 1945, **67**, 351.
- L. Hongcheng, N. Hayashi, Y. Matsumoto, H. Takatsu and H. Kageyama, *Inorg. Chem.*, 2017, **56**, 9353.
- T. Wen, D. Zhang, Q. Wen, H. Zhang, Y. Liao, Q. Li, Q. Yang, F. Bai and Z. Zhong, *Nanoscale*, 2015, **7**, 4906.
- R. E. Dunin-Borkowski, S. B. Newcomb, T. Kasama, M. R. McCartney, M. Weyland and P. A. Midgley, *Ultramicroscopy*, 2005, **103**, 67.

- 36 M. Beleggia, P. Fazzini, P. Merli and G. Pozzi, *Phys. Rev. B: Condens. Matter Mater. Phys.*, 2003, **67**, 045328.
- 37 S. Sahoo, O. Petravic, C. Binck, W. Kleemann, J. Sousa, S. Cardoso and P. Freitas, *Phys. Rev. B: Condens. Matter Mater. Phys.*, 2002, **65**, 134406.
- 38 J. A. De Toro, P. S. Normile, S. S. Lee, D. Salazar, J. L. Cheong, P. Muñoz, J. M. Riveiro, M. Hillenkamp, F. Tournus and A. Tamion, *et al.*, *J. Phys. Chem. C*, 2013, **117**, 10213.
- 39 J. De Toro, S. Lee, D. Salazar, J. Cheong, P. Normile, P. Muniz, J. Riveiro, M. Hillenkamp, F. Tournus and A. Tamion, *et al.*, *Appl. Phys. Lett.*, 2013, **102**, 183104.
- 40 Y. Sun, M. Salamon, K. Garnier and R. Averback, *Phys. Rev. Lett.*, 2003, **91**, 167206.
- 41 M. Sasaki, P. Jönsson, H. Takayama and H. Mamiya, *Phys. Rev. B: Condens. Matter Mater. Phys.*, 2005, **71**, 104405.
- 42 W. Luo, S. R. Nagel, T. Rosenbaum and R. Rosensweig, *Phys. Rev. Lett.*, 1991, **67**, 2721.